

# Strong gravitational lensing with upcoming wide-field radio surveys

Samuel McCarty<sup>1,2,\*</sup>, Liam Connor<sup>3</sup>

<sup>1</sup>*Department of Astronomy, University of Washington, Seattle, WA 98195-1580, USA*

<sup>2</sup>*Cahill Center for Astronomy and Astrophysics, MC 249-17, California Institute of Technology, Pasadena CA 91125, USA*

<sup>3</sup>*Center for Astrophysics | Harvard & Smithsonian, Cambridge, MA 02138-1516, USA*

Accepted XXX. Received YYY; in original form ZZZ

## ABSTRACT

The number of strong lensing systems will soon increase by orders of magnitude thanks to sensitive, wide-field optical and infrared imaging surveys such as Euclid, Rubin-LSST, and Roman. A dramatic increase in strong lenses will also occur at radio wavelengths. The 2000-antenna Deep Synoptic Array (DSA-2000) will detect over  $10^9$  continuum sources in the Northern Hemisphere with a high mean redshift ( $\langle z_s \rangle \approx 2$ ) and the Square Kilometer Array (SKA) will observe a large sample of extragalactic sources in the South with sub-arcsecond resolution. We forecast lensing rates, finding that the DSA-2000 will discover  $O(10^5)$  strongly lensed systems, many of which will be galaxy group and cluster lenses. We propose strategies for strong lensing discovery in the limit where the Einstein radii are comparable to the PSF angular scale, taking advantage of modern computer vision techniques and multi-survey data. We also forecast synergies with optical and infrared surveys, which will provide redshifts as well as multiwavelength information about the lens systems. Finally, we describe applications of radio strong lensing systems, including time-delay cosmography with transient and variable sources. We find that  $\sim 100$  time-variable flat-spectrum AGN discovered by the DSA-2000 could be used to constrain  $H_0$  at the percent level with the appropriate follow-up.

**Key words:** gravitational lensing: strong – radio continuum: general

## 1 INTRODUCTION

Strong gravitational lensing has a multitude of applications in astrophysics and cosmology (Treu 2010). Previously theoretical ideas have been put into practice in recent decades as the number of known lensed systems has increased and observational data have improved. For example, strongly lensed time-variable and transient sources can be used to constrain the Hubble constant,  $H_0$ , because the time delay of a multiply imaged source depends on the geometry of the Universe (Refsdal 1964). The technique is known as time-delay cosmography. With just six lensed quasar systems, the  $H_0$  Lenses in COSMOGRAIL’s Wellspring (H0LiCOW) collaboration has reported 2.4% precision on their  $H_0$  measurement, which is independent of the distance ladder and the CMB (Wong et al. 2019).

In addition to the Universe’s large-scale geometry, lensing observables are sensitive to the total mass of the deflector galaxy or cluster, allowing one to measure the spatial distribution of matter and test different dark matter models (Massey et al. 2010; Vegetti et al. 2024). Lensing magnification allows astronomers to observe objects in the distant Universe, as was pointed out at the field’s inception (Zwicky 1937). Dramatic examples have come from the James Webb Space Telescope (JWST), including a red supergiant star at  $z \approx 2.2$  that appears to be magnified by a factor of several thousand due to its proximity to caustics in a cluster lens (Diego et al. 2023).

Nearly all of these applications would benefit from a larger sample of strong lensing systems. To date, roughly  $10^3$  strong lensing systems have been discovered, most of which were identified at optical

and infrared wavelengths (O/IR). Fortunately, upcoming wide-field imaging surveys such as Euclid and The Vera C. Rubin Observatory’s Legacy Survey of Space and Time (Rubin-LSST) are each expected to detect as many as  $\sim 10^5$  strong lenses (Collett 2015). An early release of a  $0.7 \text{ deg}^2$  field from Euclid has recently affirmed these forecasts (Barroso et al. 2024). The Nancy Grace Roman Space Telescope’s 2000 square degree survey could find of order 20,000 strong lenses (Weiner et al. 2020), and many more if the proposed multi-epoch  $4\pi \text{ sr}$  survey is carried out (Han et al. 2023). An increase in the total number of lenses by two-orders of magnitude will usher in a new era of strong lensing science.

The first strongly lensed system ever discovered was co-detected at radio wavelengths (Walsh et al. 1979). The first survey for lenses, the Mit-Green Bank survey, was also in the radio (Bennett et al. 1986). Despite this, fewer than  $\sim 100$  radio lensing systems have been detected to date. This is due to the relatively small total number of known radio sources ( $\sim 10^7$ ) and the lack of wide-field imaging surveys with  $\sim$  arcsecond resolution. Both of those limitations will soon be overcome with the advent of next-generation radio survey telescopes.

The 2000-antenna Deep Synoptic Array (DSA-2000) will detect over one billion radio sources with a deep redshift distribution, most of which will be star-forming radio galaxies (SFRG) or active galactic nuclei (AGN) (Hallinan et al. 2019). The DSA-2000 is expected to see first light in 2027 with key surveys running between 2028 and 2033. Its point-spread function (PSF) will be roughly  $2''$  at the top of the 0.7–2 GHz radio band. A fifty-fold increase in the total radio source catalog is made possible by the DSA-2000’s high survey speed, driven by a large field-of-view ( $\sim 10 \text{ deg}^2$ ) and high sensitivity (the expected

\* E-mail: smmccrty@uw.edu & liam.connor@cfa.harvard.edu

system-equivalent flux density or “SEFD” is just 2.5 Jy). Its cadenced all-sky survey will map out the  $3\pi$  sr above declination  $-30^\circ$  down to 500 nJy/beam root-mean square noise (Hallinan et al. 2019). While the nominal cadence of the continuum survey is four months, certain fields may be visited more regularly, presenting an opportunity to measure lensing time delays with better temporal sampling.

The mid-frequency telescope for the square kilometre array (SKA-Mid) will consist of 197 fully steerable 13.5 m dishes (including the existing MeerKAT radio telescope), operating between 350 MHz and 15.4 GHz with a field-of-view of roughly  $1 \text{ deg}^2$  at 1400 MHz. The end of its construction is anticipated to be July 2029<sup>1</sup>. Although the SKA’s lower survey speed will result in fewer sources than the DSA-2000, the wide frequency range and long maximum baseline (150 km) will enable high-resolution imaging, an asset to strong lensing studies (McKean et al. 2015). The Next Generation Very Large Array (ngVLA) is a planned interferometer with extraordinary sensitivity covering a wide range of frequencies (1.2–116 GHz) (Selina et al. 2018a). It will be able to resolve features at milliarcseconds scales. While its broad science goals did not require optimizing the instrument for mapping speed (Selina et al. 2018b), the ngVLA will be a world-class instrument for strong lensing science.

Radio strong lensing offers distinct advantages to studies at shorter wavelengths and will complement O/IR imaging surveys. Star-forming radio galaxies and AGN can be detected to great distances, boosting the mean optical depth of radio continuum sources. Obscuration by dust in lensing galaxies is not an issue at radio wavelengths, nor is the variable “seeing” that impacts ground-based O/IR telescopes. Relatedly, the point-spread function (PSF) of a radio interferometer is directly determined by observing frequency and array configuration, allowing us to accurately forward model the instrument’s response. In the limit of a large number of antennas and a filled aperture (a “radio camera”), the deterministic PSF allows us to be more ambitious in image-plane deconvolution, enabling techniques such as superresolution (Connor et al. 2022). Radio telescopes also measure full polarization information, which is conserved under gravitational lensing (Greenfield et al. 1985; Dyer & Shaver 1992). The rotation measure (RM) of a lensed source allows one to measure the magnetic field and ionized gas properties of intervening halos (Mao et al. 2017). Finally, the larger emission regions of radio AGN render them less susceptible to microlensing by substructure in the lens, and may provide cleaner modelling of the deflector mass distribution (Birrer et al. 2024). This is critical for measuring  $H_0$  via time-delay cosmography.

There are of course several drawbacks to strong lensing studies in radio surveys, often precluding the use of standalone radio observations. For example, continuum sources will not contain redshift information, and multi-wavelength datasets or follow-up will be necessary for the majority of lensed systems at radio frequencies. Secondly, the morphology of radio lobes can mimic lensing arcs, exacerbating the already-challenging lens identification problem (consider, for example, head-tail galaxies 3C 465 or 3C 129 at redshift 2). In the case of the DSA-2000, the angular resolution is such that 75–90% of galaxy-galaxy lensing systems will be unresolved in the absence of superresolution.

In this work we seek to study radio strong lensing in upcoming interferometric surveys, and develop strategies that alleviate the drawbacks of radio lensing. We focus on the DSA-2000, first by forecasting its strong lensing rates for different source classes. We compare this with a forecast for strong lensing discovery on the SKA. Next, due to

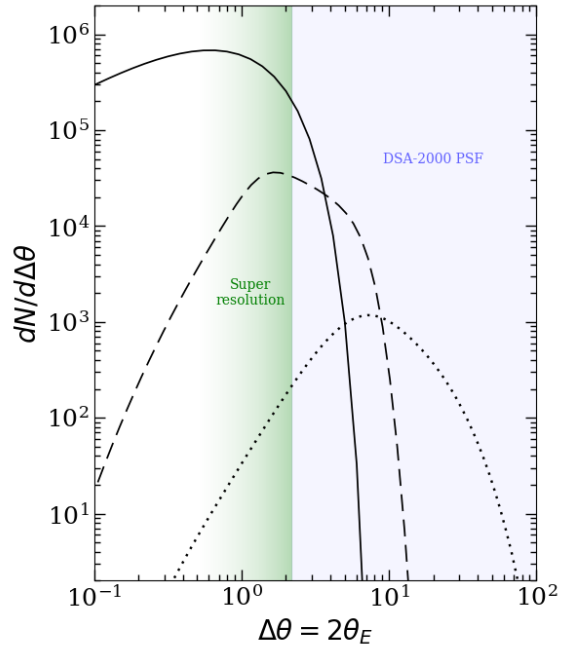


**Figure 1.** The theoretical distribution of strongly lensed image separations ( $2\theta_E$ ) from our model for galaxies (solid), galaxy groups (dashed), and galaxy clusters (dotted), assuming a DSA-2000 source redshift distribution. The portion that will be discoverable by the DSA-2000 is shown in the blue-shaded region, while the portion that could be discoverable with superresolution is shown in the green-shaded region. The galaxy group distribution is flat at the top because the density profile is constant over the entire mass range in our model.

the 2–3” PSF of the DSA-2000, we discuss methods for superresolving lensing candidates with modern computer vision techniques in order to increase the yield of strongly lensed systems. We then consider lensed time-variable and transient sources that the DSA-2000 will find and forecast constraints on  $H_0$  that can be achieved with the appropriate follow-up, as well as other applications of strong lensing.

## 2 OPTICAL DEPTH CALCULATION & EXPECTED RATES

First, we offer a simple empirical forecast based on observational data and cosmological simulations, and then offer a more detailed forward model that accounts for different source classes and the deflector population.

### 2.1 Empirical forecast

The Cosmic Lens All Sky Survey (CLASS) (Myers et al. 2003) sought to study a statistical sample of radio-loud gravitationally lensed systems. Despite significant advances in both radio instruments and lens-finding algorithms in the two decades since CLASS, the number of known radio lenses has not increased dramatically. We can use CLASS for a rough estimate of the number of lenses the DSA-2000 will find. CLASS found that a complete sample of 8,958 flat-spectrum radio point sources brighter than 30 mJy had a mean lensing optical depth of  $1.5^{+0.5}_{-0.3} \times 10^{-3}$  (Browne et al. 2003). By targeting compact sources with flat spectra, many of their objects are quasars at high redshifts, comparable to typical redshifts of DSA-discovered sources, despite the difference in flux scales. Of the

<sup>1</sup> <https://www.skao.int/en/explore/telescopes/ska-mid>

confirmed radio lenses, approximately 20% had angular separations larger than 2 arcseconds, which could be detected by the DSA-2000. Thus, a rough estimate indicates that for every 10,000 sources detected by the DSA-2000, several could be identified as strong lenses. If we assume a detection threshold of  $10\sigma$ , the number of extragalactic DSA-2000 sources becomes roughly  $5 \times 10^8$  (Section 2.3). This would result in  $O(10^5)$  new galaxy-scale radio lenses, depending on the practical signal-to-noise threshold for candidate systems.

Galaxy group and cluster scale lenses have been neglected in previous investigations of lensing statistics for upcoming surveys because they make up a smaller, but still significant, fraction of the total lenses. Additionally, lens modeling is more complicated in this regime. The dark matter halos of groups, in particular, are complex and not well-understood structures. From Oguri (2006), the number of group and cluster lenses are around 11% and 3% of the total galaxy lenses respectively (excluding sub-halo lensing). However, these systems make up a considerable portion of lens systems with angular separation of order  $1''$ , and almost all of the lenses at  $\geq 10''$ . Because the PSF of the DSA-2000 is relatively large ( $2''$  at 2 GHz and  $3.3''$  at 1.4 GHz), these lenses will make up a large fraction of the discoverable lensing systems and so must be accounted for in our investigation.

A radio group/cluster lens survey as complete as CLASS does not exist, but we can make a simple empirical estimate from the literature. The total number of galaxy scale lenses should be  $O(10^6)$  assuming  $10^9$  sources and the CLASS lensing optical depth. Taking the percentages of group/cluster lenses from Oguri (2006), we should see  $O(10^5)$  group scale lenses and  $O(10^4)$  cluster scale lenses, almost all of which will have angular separation large enough to be detected in the DSA-2000. The first and largest survey for group-scale lenses was the Strong Lensing Legacy Survey (SL2S) (Cabanac, R. A. et al. 2007). SL2S found 13 strong lens systems in the mass range of groups in  $\sim 100 \text{ deg}^2$  of the Canada France Hawaii Telescope Legacy Survey (CFHTLS), giving a rate of  $\sim 0.13 \text{ deg}^{-2}$  (Limousin, M. et al. 2009). A later publication identified at least 54 promising group lenses in  $\sim 150 \text{ deg}^2$  of the CFHTLS (More et al. 2012). However, the mean redshift of the CFHTLS sources used in SL2S is  $\langle z_s \rangle < 1$ , and we expect  $\langle z_s \rangle \approx 2$  for the DSA-2000 (see section 2.3, figure 3 below) (Coupon, J. et al. 2009). At these redshifts, we expect the lensing optical depth to be roughly  $\propto z^2$  (see equation 31 of Oguri (2019); figure 2 below). This means that we would expect to see  $\sim 10^{+6}_{-6}$  times more group lenses in the DSA-2000, for a total of  $\sim 1.1^{+0.6}_{-0.9} \times 10^5$ . Similarly, the Red Sequence Cluster Survey found 8 cluster lenses in  $\sim 90 \text{ deg}^2$  with shallower CFHT imaging, indicating  $\sim 2.6^{+1.6}_{-1.6} \times 10^4$  cluster lenses in the DSA-2000 (Gladders et al. 2003). These estimates are of the same order of magnitude as expected from Oguri (2006).

Alternatively, if we take the cross section for giant arcs from the simulations of Puchwein & Hilbert (2009), Fedeli, C. et al. (2010), and Mahdi et al. (2014), assume typical values of  $M = 1 \times 10^{14} M_\odot$ ,  $z_d = 0.5$ , and  $z_s = 2$ , we can calculate a rough estimate of the cluster lensing optical depth at  $z_s = 2$ . The cross sections at these values are all on the order of  $10 \text{ arcsec}^2$ . From Böhringer, Hans et al. (2017), the number density at  $M = 1 \times 10^{14} M_\odot$  is approximately  $\geq 1 \times 10^{-6} \text{ Mpc}^{-3}$ , and after multiplying by the differential coming volume at  $z_s = 2$  and sky coverage of the DSA-2000 we get  $\approx 5 \times 10^{-5}$  for all three simulations. When taking into account that this is the cross-section for giant arcs only, this means we should see several tens of thousands of cluster lenses in the DSA-2000, in good agreement with the previous estimates.

We also make an empirical estimate of the rate of lensed transients

in the DSA-2000. These objects are of particular interest for  $H_0$  measurements but are much harder to forward model because of the lack of observational data. We can use data from the Very Large Array Sky Survey (VLASS), which is currently the most comparable survey to the DSA-2000, for a simple estimate (Lacy et al. 2020). The determined log rates of supernovae (SNe) and tidal disruption events (TDEs) in  $\text{deg}^{-2}\text{yr}^{-1}$  are  $-1.91^{+0.15}_{-0.16}$  and  $-2.85^{+0.28}_{-0.38}$  respectively (Dong et al. 2024 in prep). If we assume that the total number of observable sources scales as  $S_{\text{min}}^{-1.5}$ , the value for a Euclidean universe, and that the flux limit of VLASS is  $0.7 \text{ mJy}$  ( $10\sigma$  from Lacy et al. (2020)), the DSA-2000 should find  $\sim 200$  more sources of each type above  $20 \mu\text{Jy}$ , which is a  $10\sigma$  detection in a single epoch of the DSA-2000. We can also assume a lensing optical depth of  $1 \times 10^{-4}$  and a magnification bias of 2, which are typical for the low redshifts at which we expect to detect transients. Because typical radio rise times of TDEs are on the order of  $10^3$  days the cadence of the DSA-2000,  $\sim 1/3 \text{ yr}$ , is fast enough to catch most TDEs (Cendes et al. 2023). Scaling for the sky coverage of the DSA-2000, and the cadence for SNe, gives a total yield of  $5^{+2}_{-1} \text{ yr}^{-1}$  and  $0.6^{+0.5}_{-0.3} \text{ yr}^{-1}$  lensed sources per year for SNe and TDEs respectively. Applying a similar estimate of the lensed rate of GRB afterglows using the predictions of Ghirlanda et al. (2013, 2014) gives a rate much less than 1 per year, and so we ignore them in the rest of this investigation.

Further, Yao et al. (2023) find a volumetric rate of optically selected TDEs of  $290^{+60}_{-130} \text{ Gpc}^{-3} \text{ yr}^{-1}$ . Cendes et al. (2023) find that  $\approx 50\%$  of optically selected TDEs emit in the radio on longer timescales. Because there are likely TDEs that emit in radio but not the optical, we take  $50\%$  of the optically selected rate to be a conservative estimate. The luminosities of the TDEs in the sample from Cendes et al. (2023) are  $\sim 10^{37} - 10^{39} \text{ ergs/s}$ , but they note that many of these are likely a lower limit because most of the TDEs still had rising emission at the time of observation. Given this, the DSA-2000 should be able to detect this rate of TDEs out to  $z \approx 0.5$ , which, when combined with the same optical depth and magnification bias as above, gives  $0.8^{+0.2}_{-0.4} \text{ yr}^{-1}$  lensed TDEs. This number is in good agreement with the previous estimate, so in general, we expect to see about 1 lensed TDE per year in the DSA-2000. However, as noted before, this is a conservative estimate, and there is reason to believe that the actual rate of total and lensed TDEs in the DSA-2000 might be significantly higher. Additionally, because many of the TDEs will be bright in multiple epochs, the DSA-2000 could detect them well below the  $20 \mu\text{Jy}$  limit, which would increase the rate by a large factor.

The DSA-2000 will also discover tens of thousands of distant fast radio bursts (FRBs) (Petroff et al. 2019; Cordes & Chatterjee 2019), some of which will be strongly lensed (Connor & Ravi 2023). The key advantage to using FRBs for time-delay lensing is that their short duration and coherence allows for exceptional precision on the gravitational lensing time delay (Wucknitz et al. 2021). Radio telescopes can preserve phase information about the electromagnetic waveform at nanosecond sampling, which means microlensing signals can be searched for at ultrashort timescales (Leung et al. 2022; Kader et al. 2022). However, for cosmological lensing time delays longer than a pointing (i.e. deflectors more massive than  $\sim 10^8 M_\odot$ ), one needs to catch the lensed images by pointing at the same patch of sky when it arrives. We do not forecast lensed FRB rates here and point the reader to previous estimates (Connor & Ravi 2023).

## 2.2 Lens Model

Next, we build a forward model based on the lens and source distributions. Following Yue et al. (2022b), the lensing optical depth for a

	All sources	SFRG	Total AGN	Blazars	Transients (yr <sup>-1</sup> )
Total	8.6±3.0×10 <sup>8</sup>	8.0±2.8×10 <sup>8</sup>	5.5±1.9×10 <sup>7</sup>	1.8±0.6×10 <sup>7</sup>	5.2±1.8×10 <sup>4</sup>
Galaxy lens	8.3±3.1×10 <sup>4</sup>	8.1±3.1×10 <sup>4</sup>	2.1±0.8×10 <sup>3</sup>	4.8±1.8×10 <sup>2</sup>	
Group lens	3.8±2.5×10 <sup>4</sup>	3.7±2.5×10 <sup>4</sup>	1.0±0.6×10 <sup>3</sup>	5.1±3.4×10 <sup>2</sup>	~ 3
Cluster lens	7.5±3.2×10 <sup>3</sup>	7.3±3.1×10 <sup>3</sup>	1.8±0.8×10 <sup>2</sup>	1.0±0.4×10 <sup>2</sup>	

**Table 1.** Total sources above  $10\sigma_n$  and expected number of discoverable lensing events by deflector type in the DSA-2000, organized by source classes. Blazars are both FSRQs and BLLacs and transients here include ccSNe and TDEs.

singular isothermal sphere (SIS) is

$$\tau(z) = \int_0^{z_s} dz_d \int d\sigma \Phi(\sigma, z_d) \frac{d^2 V_c}{d\Omega dz_d} \pi \theta_E(\sigma, z_d, z_s)^2 D_d^2, \quad (1)$$

where  $z_d$  is the redshift of the deflector,  $z_s$  is the redshift of the source,  $\sigma$  is the 1D velocity dispersion of the deflector,  $\Phi(\sigma, z_d)$  is the velocity dispersion function (VDF) of the deflectors,  $\frac{d^2 V_c}{d\Omega dz_d} = (1+z_d)^3 c \frac{dV_c}{dz_d}$  is the differential comoving volume,  $\theta_E(\sigma, z_d, z_s)$  is the Einstein radius, and  $D_d$  is the angular diameter distance at the deflector redshift. The SIS model (or its elliptical generalization) has been shown to replicate the properties of early-type galaxies, which make up the majority of galaxy lenses (e.g. Gavazzi et al. (2007); Koopmans et al. (2009); Li et al. (2018)), and is a widely used model for galaxy strong lensing statistics (e.g. Oguri & Marshall (2010); Collett (2015); Yue et al. (2022a)). For a SIS, the Einstein radius becomes

$$\theta_E = 4\pi \left(\frac{\sigma}{c}\right)^2 \frac{D_{ds}}{D_s}, \quad (2)$$

where  $D_{ds}$  is the angular diameter distance from the deflector to the source and  $D_s$  is the angular diameter distance from the observer to the source. We use the analytical VDF from Yue et al. (2022b) to model the galaxy deflector population, which they show to be in good agreement with observations. We include a sharp exponential cutoff on the VDF at  $300 \text{ km s}^{-1}$  which corresponds roughly to the transition between galaxies and galaxy groups.

An important ingredient in the calculation is the magnification bias, which increases the rate of lensed sources by about a factor of two at low redshifts, or by orders of magnitude at high redshifts. The general magnification bias is

$$B = \frac{\int_{\mu_{\min}}^{+\infty} d\mu p(\mu) N(> L_{\min}/\mu)}{N(> L_{\min})}, \quad (3)$$

where  $\mu$  is the magnification of a lensed source,  $p(\mu)$  is the probability distribution of the magnification,  $L_{\min}$  is the smallest observable luminosity, and  $N(> L_{\min})$  is the number of sources brighter than  $L_{\min}$ . For SIS,  $\mu_{\min} = 2$  for the total magnification of the multiple images. A SIS will produce only two multiple images; if the separation of the multiple lens images is large enough to be resolved then  $p(\mu) = \frac{2}{(\mu \pm 1)^3}$  describes the magnification of the fainter (+) and brighter (-) image (Wyithe et al. 2001). If the lens is not resolved then  $p(\mu) = \frac{8}{\mu^3}$  is the total magnification of both images. Combining  $B$  and  $\tau$  for the total fraction of lensed sources:

$$F_{\text{lensed}} = \frac{B\tau}{B\tau + B'(1-\tau)}, \quad (4)$$

where  $B'$  is the magnification bias of sources that are not lensed, which is assumed to be unity.

While the SIS model describes deflector galaxies well, the mass distributions of galaxy groups and clusters behave differently. It has been traditionally thought that in the limit of large mass and large image separation, i.e. clusters, the distribution will be dominated by the dark matter halo, generally following the Navarro-Frenk-White (NFW) profile (Navarro et al. 1997). Recent works suggest that NFW profiles may not be the most accurate representation of large dark matter halos (e.g. Klypin et al. (2016)), but we use them here because they are a decent approximation and their lensing properties are well known. Regardless, for the mass range of groups, it is clear that some intermediate model between SIS and NFW is necessary (Williams et al. 1999; Oguri 2006; More et al. 2012). In a SIS the density  $\rho \propto r^{-2}$ , while the NFW has  $\rho \propto r^{-1}$  on small scales and  $\rho \propto r^{-3}$  on larger scales. The shallower NFW profile has a significantly smaller cross-section than SIS. Oguri (2006) include the effects of baryon cooling and the large elliptical galaxies found at the center of most halos in their model, which will steepen the central density profile and increase the cross-section of halos (especially for groups). Without introducing these complexities, we can steepen the inner profile of halos by modeling them as Generalized NFW (GNFW) profiles. The GNFW is:

$$\rho(r) = \frac{\rho_s r_s^3}{r^\alpha (r + r_s)^{3-\alpha}}, \quad (5)$$

where  $r_s$  is the scale radius and  $\rho_s$  is the scale density (Li & Ostriker 2002). When  $\alpha = 1$  we have the standard NFW. When  $\alpha = 2$  the profile resembles an SIS below the scale radius and when  $1 < \alpha < 2$  the inner profile is somewhere in between. Using weak lensing and stellar kinematics, Wang et al. (2023) find the inner dark matter density profiles of group ( $10^{13} M_\odot \leq M < 10^{14} M_\odot$ ) and cluster ( $M \geq 10^{14} M_\odot$ ) halos are  $1.82_{-0.25}^{+0.15}$  and  $1.48_{-0.41}^{+0.2}$  respectively. Similarly, Mandelbaum et al. (2006) find that the total inner profiles of groups with mass  $\sim 2.5 \times 10^{13} M_\odot$  are decently described by a power-law of slope  $\gamma_{\text{tot}} = 1.85$ . However, at  $\sim 7 \times 10^{13} M_\odot$  they are less steep than 1.85 and closer to the traditional NFW. Newman et al. (2013) find  $\gamma_{\text{tot}} = 1.16_{-0.12}^{+0.10}$  for the inner profile of clusters with  $M = 0.4 - 2 \times 10^{15} M_\odot$ , and Newman et al. (2015) find the total inner profile slope  $\gamma_{\text{tot}} \approx 1.7$  while the dark matter slope  $\alpha \approx 1.35$  for galaxy groups with  $\langle M \rangle \approx 10^{14} M_\odot$ . In this work, we use the GNFW profile with  $\alpha = 1.6$  to model groups and  $\alpha = 1.2$  to model clusters. The resulting GNFW profiles will capture the inner profile well, which is crucial for lensing, and also converge to the standard NFW profile at large radii where we expect the density to be dominated by dark matter (e.g. figures 3 and 4 of Wang et al. (2023)). The GNFW is completely parameterized by  $\alpha$ , its mass  $M$ , and the concentration parameter,  $c$ , from which  $r_s$  and  $\rho_s$  can be determined as in Li & Ostriker (2002). The mass and  $c$  are correlated with some scatter,

we use the relationship presented by [Dutton & Macciò \(2014\)](#) for  $c_{200}$ . The scatter in  $c$  is lognormal with  $\sigma_{\log c} = 0.11$ . We include an additional factor of  $(2 - \alpha)$  as in [Oguri et al. \(2001\)](#) to correct for the generalized form of the NFW which ensures that the radius at which the logarithmic density slope becomes  $-2$  is the same as in the standard NFW for all  $\alpha$ . The lensing power of the GNFW halo is very sensitive to  $c$  and its scatter, so having an accurate relationship is important; early investigations tend to overestimate these values.

The lens equation relates a position on the lens plane,  $x$ , to a position on the source plane,  $y$ , which for a GNFW profile is

$$y = x - \mu_s \frac{g(x, \alpha)}{x}, \quad (6)$$

where

$$\mu_s = \frac{4p_s r_s}{\Sigma_{cr}}, \quad \Sigma_{cr} = \frac{c^2}{4\pi G} \frac{D_s}{D_d D_{ds}}, \quad (7)$$

and  $g(x, \alpha)$  is the same as in [Li & Ostriker \(2002\)](#). The lens equation has three solutions inside the radial caustic,  $y_{cr}$ , which are the multiple images produced by the GNFW profile. The cross-section for lensing is the area in the source plane in which multiple images will be produced, i.e. the area inside the radial caustic. This is approximated as:

$$\sigma(M, z) \approx \pi y_{cr}^2 r_s^2 \quad (8)$$

where  $y_{cr} = -y(x_{cr})$  and  $x_{cr}$  is the location of the minimum of equation 6 ([Li & Ostriker 2002](#)). The image separation is given by the separation between the outer two images, which can be approximated as

$$\Delta\theta \approx \frac{2x_0 r_s}{D_d} \quad (9)$$

where  $x_0$  is the position of the tangential critical curve and can be found as the root of equation 6 ([Li & Ostriker 2002](#)). The Einstein radius is just half of the image separation,  $\theta_E = \Delta\theta/2$ .

In general, because our GNFW profiles are shallower than a SIS, they will be worse at producing multiple images but significantly better at magnifying. This is particularly sensitive to  $c$ , which defines the shallowness of the GNFW profile. For our concentration parameters, especially at high redshift, we expect the magnifications from the GNFWs to be several times larger than from SIS ([Wyithe et al. 2001](#)). To calculate the magnification bias for a GNFW profile, we first determine the minimum magnification as ([Li & Ostriker 2002](#)):

$$\mu_{\min} \approx 2 \frac{x_0}{y_{cr}}. \quad (10)$$

With  $\mu_{\min}$  we calculate B according to equation 3 with ([Li & Ostriker 2002](#)):

$$p_{\text{nfw}}(\mu) = 2 \frac{\mu_{\min}^2}{\mu^3}. \quad (11)$$

The minimum magnification for both the first and second brightest image can be approximated as half of the total minimum magnification ([Oguri et al. 2002](#)). Substituting  $\mu_{\min} = 2$  into equation 11 recovers the total magnification distribution for SIS.

To model the populations of galaxy groups and clusters we determine Mass Functions (MF) from the CosmoDC2 synthetic catalogue [Korytov et al. \(2019\)](#). For simplicity, we define a galaxy group as a

system with mass  $10^{13} M_\odot \leq M < 10^{14} M_\odot$  and a galaxy cluster as  $M \geq 10^{14} M_\odot$ . We find all dark matter halos in a redshift interval where the mass of the halo and its constituent galaxies fall in these ranges. We fit Schechter functions to the binned results. The fitted functions match the results of [Böhringer, Hans et al. \(2017\)](#) well at  $z = 0$  and show a realistic decline in the mass function towards higher redshift. To calculate the optical depth, we replace  $\pi\theta_E(\sigma, z_d, z_s)^2 D_d^2$  in equation 1 with equation 8,  $\Phi(\sigma, z_d)$  with the CosmoDC2 MF, and integrate over  $M$  instead of  $\sigma$ .

While equation 4 gives the total fraction of lensed sightlines, we are more interested in the number of discoverable lenses. We define a lens as discoverable if its image separation  $\Delta\theta = 2\theta_E$  is larger than 2/3rds of the FWHM of the PSF of the survey instrument (as in [Oguri & Marshall \(2010\)](#); [Yue et al. \(2022a\)](#)) so that multiple images can be resolved. Further, for point-like sources (i.e. flat-spectrum sources and transients), we require the second faintest image to be detectable at  $10\sigma$  confidence so that the lens can be identified. To account for this we integrate equation 1 from  $\sigma_{\min}$  (or equivalently  $M_{\min}$  for groups and clusters) corresponding to  $\theta_{E\min}$  and use the magnification bias of the fainter image. The second image from a SIS will often be demagnified, so the magnification bias of the fainter image is typically a bit less than 1, while the magnification bias of the fainter image from an NFW will be about half of the total. For SFRGs and SS-AGN, which in general have extended emission regions, the lensed images will be stretched into arcs and rings, and so for this case we require the brightest image to be detectable at  $10\sigma$  confidence (using the magnification bias of the brightest image) because only one arc is needed to identify a lens.

The image separation distribution predicted by our model and the lensing optical depths for galaxies, groups, and clusters are shown in Figures 1 and 2 respectively. We see that the optical depth increases rapidly at small redshift as expected, and approximately matches the estimates given in Section 2.1. The galaxy lens optical depth is smaller than the approximation from [Oguri \(2019\)](#). The discoverable optical depth, limited by the PSF of the DSA-2000, is significantly smaller than the total optical depth for galaxies but similar to the total for groups and clusters. The image separation distribution matches the results of [Oguri \(2006\)](#) well despite the simpler model. As expected, galaxies lie mostly at  $\Delta\theta \approx 1''$ , while groups and clusters correspond to  $\Delta\theta \approx 10''$  and  $10'' \lesssim \Delta\theta \lesssim 100''$  respectively. The largest uncertainty is in the model of groups, as our simple model does not capture many of the complexities of halo profiles and is constant over the whole mass range. Further, varying  $\alpha$  between 1 and 2 creates a significant change in the calculated group optical depth. On the other hand, there is inherent uncertainty in all three models from the assumption of spherical symmetry. Using SIS instead of Singular Isothermal Ellipsoids (SIE) for galaxies will overestimate the galaxy lens population by  $\sim 10\%$ , which is corrected for in our final numbers ([Yue et al. 2022b](#); [Ferrami & Wyithe 2024](#)). Introducing ellipticity will similarly reduce the cross-section of NFW profiles.

We do not account for effects such as sub-halo lensing or line-of-sight structures and lens environments. It is shown in [Oguri \(2006\)](#) that a significant fraction of lenses, roughly half for groups and clusters and 10% for galaxies, come from lensing by sub-halos. The environment around these sub-halos boosts their lens capabilities and image separations. At least one of the CLASS lenses is caused by a galaxy within a galaxy group ([Auger et al. 2007](#)). In the context of cluster lensing, this is termed galaxy-galaxy strong lensing (GGSL) and it is reported that observational numbers of GGSL exceed expectations of the  $\Lambda$ CDM model ([Meneghetti, Massimo et al. 2022](#); [Tokayer et al. 2024](#)). This means that we are likely underestimating the number of lenses in the image separation range of galaxy scale

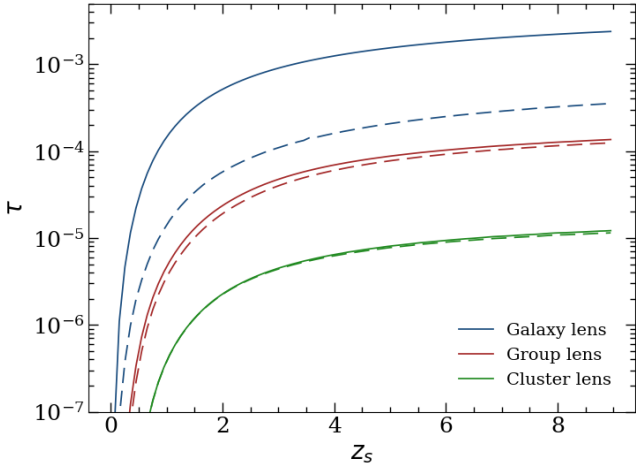


**Figure 2.** Lensing optical depth vs. redshift without magnification bias. Solid lines are the total optical depth while dashed lines are the optical depth for lenses discoverable by the DSA-2000.

lenses. However, most of these will be below the discoverable limit of the DSA-2000. Further, it is well known that intervening masses along the line of sight between the deflector and the observer could increase the probability of multiple imaging by a significant fraction, especially at high source redshifts, which we also neglect in this study (Fleury et al. 2021). Because these higher-order aspects of the model are likely to *increase* the number of lenses, for the purpose of this paper it is safe to ignore them.

### 2.3 Source Populations

The other important piece of the model is the population of the sources. The DSA-2000 will map  $\sim 30,000 \text{ deg}^2$  of the sky to a combined  $\sigma_n = 500 \text{ nJy/beam}$  rms noise (Hallinan et al. 2019). Matthews et al. (2021) presents detailed radio source counts from the MeerKat DEEP2 image, including direct source counts above  $10 \mu\text{Jy}$  and statistical counts extrapolating below  $10 \mu\text{Jy}$ . They find that for sources  $< 10 \mu\text{Jy}$ , the differential source count is significantly flatter than Euclidean. Scaling for the  $30,000 \text{ deg}^2$  footprint of DSA-2000’s continuum survey and integrating down to a minimum flux density  $S = 2.5 \mu\text{Jy}$  for a  $5\sigma_n$  combined detection gives an expected total source count of  $1.45^{+0.25}_{-0.10} \times 10^9$ , while for  $S \geq 5 \mu\text{Jy} = 10\sigma_n$  that number is  $8.6^{+1.1}_{-0.4} \times 10^8$ .

To get redshift distributions for different source classes, we model the Star-Forming Radio Galaxy (SFRG) and Active Galactic Nucleus (AGN) populations using the luminosity functions (LF) from the Tiered Radio Extra-galactic Continuum Simulation (T-RECS) (Bonaldi et al. 2018). These have been shown to match observations out to high redshift. Following Bonaldi et al. (2018), we divide the AGN into three sub populations: Flat Spectrum Radio Quasars (FSRQ), BL-Laceratae (BLLac), and Steep Spectrum AGN (SS-AGN). We expect SFRGs to make up roughly 95% of all of the sources in any synoptic radio survey, and BLLacs to be the rarest source.

From the LF we calculate the number of sources in a redshift interval as

$$n(z)dz = \int_{L_{\min}(z)} \Phi(L, z) d\log L \times \frac{d^2V_c}{d\Omega dz d} \times dz \times \Omega_{\text{survey}} \quad (12)$$

where  $\Omega_{\text{survey}}$  is the sky coverage of the survey in steradians ( $\approx 3\pi$  for the DSA-2000) and  $\Phi(L, z)$  is the LF of the source population.

$L_{\min}(z) = \frac{4\pi D_L^2}{(1+z)^{1+\alpha}} S_{\min}$  is the minimum observable luminosity at a redshift  $z$ , where  $D_L$  is the luminosity distance,  $\alpha$  is the spectral index of the source population,  $S_{\min}$  is the  $10\sigma_n$  flux sensitivity of the DSA-2000, and the factor  $(1+z)^{-(1+\alpha)}$  is the standard cosmological radio K-correction. We scaled the total number of sources in the LF model to match the observational prediction from the DEEP2 image given above.

In addition to SFRGs and AGN, we build a model for radio SNe. To date, only  $\sim 100$  radio core-collapse supernovae (ccSNe) have been detected and the first Type Ia radio supernova was detected last year (Bietenholz et al. 2021; Kool et al. 2023). To model the expected rate of radio ccSNe we follow Lien et al. (2011). Because ccSNe are short-lived, the rate of ccSNe is closely related to the cosmic Star Formation Rate (SFR), which has been observational measured to high redshift and accuracy. We use the ccSNe radio luminosity distribution of Bietenholz et al. (2021), which is more complete than the one in Lien et al. (2011). The best-fit distribution is log-normal and incorporates all known radio ccSNe as well as radio non-detections of supernovae. Bietenholz et al. (2021) note that their data is likely biased towards radio detections, finding that 30% of all ccSNe are detected in the radio. We divide the total number of radio ccSNe in the model by 3 to get a more conservative 10% as in Lien et al. (2011). From the luminosity distribution, we determine the number of radio ccSNe at each redshift above the flux limit of the DSA-2000. Because the SNe observations used in Bietenholz et al. (2021) have frequencies ranging from 2-10 GHz, there is uncertainty when converting to 1.4 GHz. We correct  $L_{\min 6\text{GHz}}(z) = L_{\min 1.4\text{GHz}} \left(\frac{6}{1.4}\right)^\alpha$ , where we assume  $\alpha = -0.7$  for the synchrotron emission of radio ccSNe. Further, because radio ccSNe have a mean rise time of  $\log_{10}(t_{\text{rise}}) = 1.7$  days (Bietenholz et al. 2021), we use the single epoch flux limit of the DSA-2000 and account for the DSA-2000’s cadence. The rms noise for a single epoch is  $\sigma_n = 2 \mu\text{Jy/beam}$ , so a  $10\sigma_n$  detection is  $20 \mu\text{Jy}$ . The cadence will be  $\sim 4$  months, so conservatively we will detect 1/3 of the radio ccSNe per year. None of the known radio ccSNe have luminosities above  $10^{29} \text{ erg s}^{-1} \text{ Hz}^{-1}$ , but given the wide spread we expect that the highest luminosities could be several times larger. Because of this we set an exponential cutoff at  $10^{30} \text{ erg s}^{-1} \text{ Hz}^{-1}$ , which we can expect to see out to about  $z \approx 1.5$  in a single epoch of the DSA-2000.

The predicted redshift distributions of SFRGs, AGN, and ccSNe from our model are shown in Figure 3 and compared to the expected distribution of Rubin-LSST sources. As expected, the total source count is dominated by SFRGs until high redshift. Blazars, meaning both FSRQs and BLLacs, are the AGN that will be most useful for time delay measurements, which is explored in Section 5.1. These are the most common sources at very high redshift. We expect the DSA-2000 to probe much higher redshifts than the Rubin-LSST because radio emission is much less susceptible to intervening gas or seeing. This is one of the reasons that the DSA-2000 will be effective at lens finding. The total number of expected sources of each type in a DSA-2000 all-sky survey with a  $10\sigma_n$  detection are listed in the first row of Table 1.

### 2.4 Expected rates

The final results of our model are shown in Table 1. The results agree quite well with the empirical estimates given in Section 2.1. As expected from CLASS there are roughly  $10^6$  total galaxy scale lenses contained in the DSA-2000 all-sky survey, less than 10% of

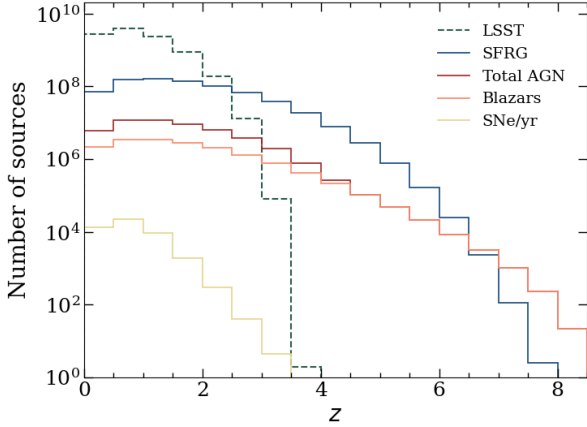


**Figure 3.** Expected source redshift distribution for the DSA-2000 from the model of Section 2.3. Blazars refers to both FSRQs and BLLacs. The distribution for Rubin-LSST is taken from [Alonso & Ferreira \(2015\)](#).

which will be discoverable. The total number of group and cluster lenses are about 10% and 2% of the galaxy number respectively, which is consistent with [Oguri \(2006\)](#). Roughly half of the group and cluster lenses will be discoverable, leading to them making up about a third of the total discoverable lenses, a significant fraction. [Yue et al. \(2022a\)](#) find that the Rubin-LSST will discover about 2000 lensed QSOs; our number is similar. This is a result of the competing mechanisms of the DSA-2000 detecting many more at higher redshifts and simultaneously being able to discover a smaller fraction because of the PSF size. The main purpose of [Yue et al. \(2022b\)](#) is to investigate the discrepancy between the fraction of lensed high redshift ( $z_s \geq 5$ ) quasars in observations ( $\sim 0.2\%$ ) and previous predictions ( $\sim 4\%$ ). [Yue et al. \(2022b\)](#) find  $\sim 0.4\text{--}0.8\%$  with their model, and we have  $\sim 0.3\%$ , which is consistent. The number of discoverable lensed ccSNe per year in the DSA-2000 from the full model is about 2, which is of the same order of magnitude as the empirical VLASS estimate. [Oguri & Marshall \(2010\)](#) conclude that Rubin-LSST will find roughly 8 SNe per year. We expect there to be less lensed SNe at radio wavelengths because not all SNe emit in the radio and the radio emission is weaker than in other wavelengths. The redshift distribution of the deflectors and sources is shown in Figure 4. Almost all deflectors are at  $z_d < 3$  and most are at  $z_d \approx 1$ , consistent with [Oguri & Marshall \(2010\)](#); [Collett \(2015\)](#); [Yue et al. \(2022a,b\)](#). This justifies the use of the CosmoDC2 catalog, which is limited to  $z < 3$ , to determine the MF of groups and clusters.

We also run the simulation for the survey specs of the SKA-mid and VLASS. The main differences are the sensitivity and resolution. The expected rms noise of the SKA-mid at 1.4 GHz will be  $\sigma_n = 2 \mu\text{Jy}/\text{beam}$ , and the PSF size will be about  $0.4''$  ([Braun et al. 2019](#)). From the DEEP2 source counts, the SKA-mid should find about  $3 \times 10^8$  sources above  $10\sigma_n$ . With this, our model predicts that the SKA-mid should see  $1.8 \pm 0.7 \times 10^5$ ,  $1.8 \pm 1.2 \times 10^4$ , and  $2.7 \pm 1.1 \times 10^3$  galaxy, group, and cluster lenses, given the same discoverability limit defined in Section 2.2. Despite less depth leading to around a third of the total galaxy lenses, the PSF of the SKA-mid is such that it will resolve over half of them, resulting in about twice as many discoverable galaxy lenses as in the DSA-2000. The SKA-mid will find fewer group and cluster scale lenses than the DSA-2000 because sensitivity is more important for discovering these systems

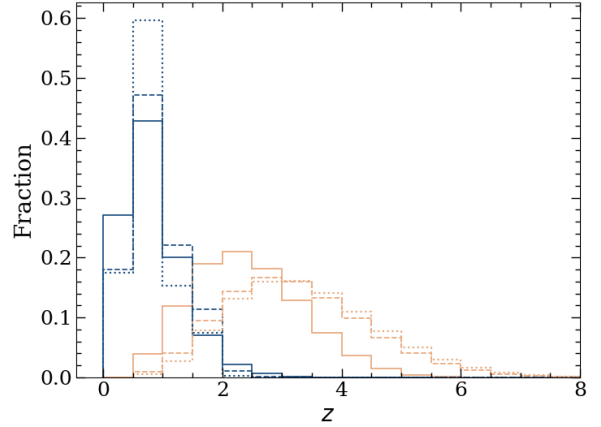


**Figure 4.** Redshift distribution of the deflectors (blue) and sources (orange) for galaxies (solid), groups (dashed), and clusters (dotted) expected in the DSA-2000 with magnification bias.

than angular resolution. In addition, we expect about 14 lensed radio ccSNe per year in an SKA-mid all-sky survey. [McKean et al. \(2015\)](#) estimate  $\sim 3 \times 10^5$  lenses in an SKA-mid all-sky survey with  $\sigma_n = 3 \mu\text{Jy}/\text{beam}$  and a lens detection limit of  $15\sigma_n$  and  $>0.3''$ . This is slightly more optimistic than our forecast, but broadly consistent. VLASS has  $\sigma_n = 70 \mu\text{Jy}/\text{beam}$  combined and an angular resolution of  $2.5''$  ([Lacy et al. 2020](#)). The DEEP2 source counts indicate that we should expect  $\sim 5 \times 10^6$  sources above  $10\sigma_n$  in VLASS ([Lacy et al. \(2020\)](#) estimate  $5.3 \times 10^6$  above  $5\sigma_n$ ). With these numbers, we estimate that there should be about 300 discoverable lenses in the full sky survey. As VLASS enters its epoch 3, many of these lenses are likely already in the data (several have recently been identified ([Martinez et al. 2024](#))).

### 3 LENS DISCOVERY

#### 3.1 Superresolution

In the past decade, tremendous progress has been made by the computer vision community with respect to the classical ill-posed inverse problems. These include deblurring ([Zhang et al. 2022](#)), deconvolution and superresolution ([Alzubaidi et al. 2021](#)), and image inpainting ([Yu et al. 2018b](#)). Nearly all of these advances were borne out of the deep learning revolution, as efficient neural network architectures and training strategies have enabled powerful learning-based tools for machine vision.

Astronomy naturally lends itself to these tools because sparse sampling and ill-posedness arise in many astronomical imaging and reconstruction contexts, especially in interferometry. Several groups have begun developing machine learning methods for interferometric image reconstruction ([Connor et al. 2022](#); [Aghabiglou et al. 2024](#); [Mars et al. 2024](#)). One reason this approach is suitable for radio astronomy is that the PSF of an array is given deterministically by the spatial distribution of antennas and the observing frequency: The on-sky response of an interferometer is the 2D Fourier Transform of its sampling in UV-space (the aperture plane). Therefore, prior physical knowledge of the PSF can be incorporated in the model either via training data ([Connor et al. 2022](#)) or fed directly to the network itself ([Mars et al. 2024](#)). This is not the case in ground-

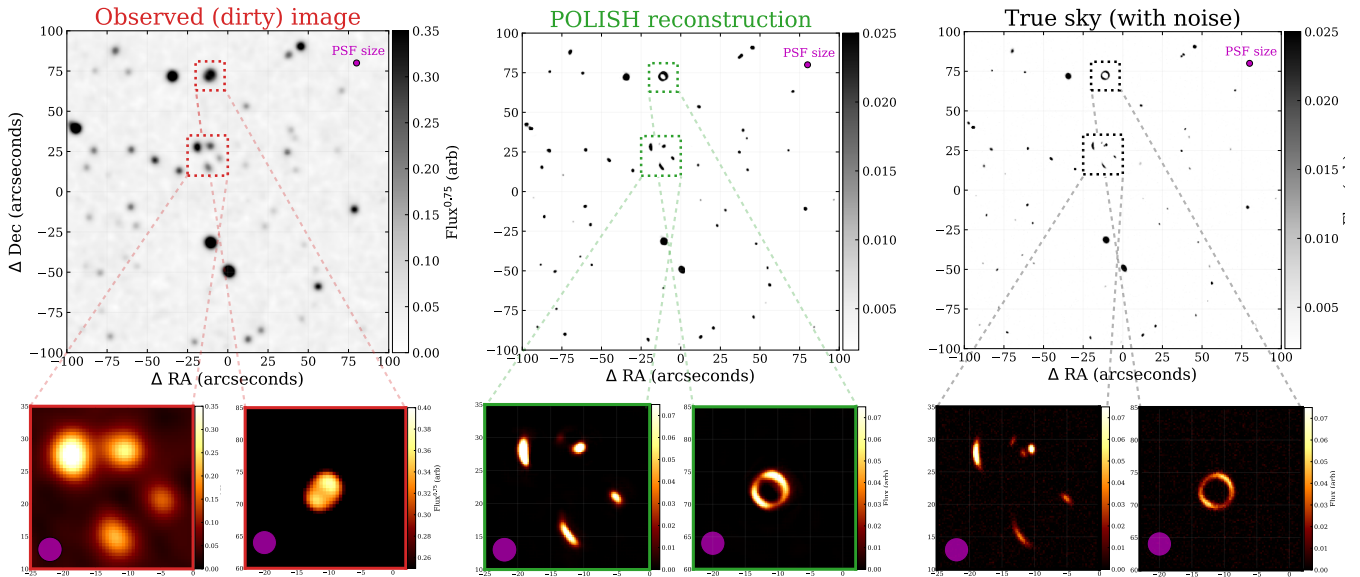


**Figure 5.** An example of superresolution image reconstruction on radio strong lenses. The simulated sky model is a mix of star-forming radio galaxies and AGN point sources. We randomly select 5% of sources to be strongly lensed. The artificially high value ensures that we have several lensing examples to reconstruct. The left panel shows a  $3.3' \times 3.3'$  region observed (i.e. the “dirty image”) with the DSA-2000 full-band PSF (size shown with mauve circle) without any deconvolution. The middle panel is a reconstruction of that field with the POLISH algorithm. The rightmost panel is the true sky. The dirty images have been gamma encoded with  $Flux^{0.75}$  with a value range of the inset figures chosen to highlight structure. In this toy example, strong lensing systems with Einstein radii below the PSF scale can be identified.

based optical astronomy where “seeing” and complex optics mean the PSF is not known a priori.

As a simple demonstration, we use the super-resolution and image-plane deconvolution method POLISH to show how strong lenses with image separations below the PSF scale can be recovered with machine learning. POLISH is a supervised machine learning model that learns the mapping between the true sky and observed images (the “dirty image” in radio parlance) (Connor et al. 2022). It uses the Wide Activation for Efficient and Accurate Image Super-Resolution (WDSR) architecture (Yu et al. 2018a), but any super-resolution neural network could be swapped in (e.g., a standard U-Net or the Efficient Super-Resolution Transformer (Lim et al. 2017)).

We have trained a POLISH network on forward-modelled synthetic data using a DSA-2000 PSF averaged over the whole band, resulting in an angular resolution of  $\sim 3.3''$ . This is worse resolution than the top of the band, where many strong lenses could be found, but we offer this as a toy example. The sky model is described in Connor et al. (2022), with the addition of strongly lensed galaxies in both the training and validation set. In Figure 5 we show an example validation image that contains multiple lenses. Lensed systems that are undetected in dirty image, including both arcs (left inset panels) and Einstein rings (right inset panels), are identifiable in the POLISH reconstruction. In the future, we plan to develop super-resolution methods explicitly for lens finding, but we take this as a promising sign that the DSA-2000 will be able to find systems with  $\theta_E \gtrsim 0.5''$ .

### 3.2 Identification

The first major hurdle for strong lensing science with DSA-2000 and other surveys is identification. The large number of sources produced by these surveys makes visual inspection by experts impossible. Despite much work on automated lens discovery (see Lemon et al.

(2023) for a review), little effort has been spent on identification in the radio. On the one hand, radio lens images are made cleaner by the lack of radio emission from the massive quiescent galaxies that make up the deflector population. However, the large, extended lobes of radio galaxies can easily be misidentified as lensing features. Further, color and photometric redshift information from UV and optical surveys have traditionally played a role in lens identification, despite being a foreground to the morphology of the lensed source.

Catalog-level searches, where large cuts are made based on certain features before a smaller subset is visually inspected, have been successful in the past. CLASS selected for flat spectrum radio sources ( $\alpha > -0.5$ ) (Myers et al. 2003). This had the advantage of picking out only blazars, whose radio emission is dominated by a small compact core, thus eliminating any confusion with intrinsic structure. A similar strategy would likely be effective in the DSA-2000. However, dedicated follow up of all of these sources, as in the  $\sim 11,000$  blazars in the initial CLASS sample, will be impossible. Similarly, a visual inspection of even a small subset of the  $O(10^7)$  blazars expected in the DSA-2000 is ambitious (hence the need for intermediate automated steps in the identification pipeline). Still, targeting flat spectrum sources could increase the yield of any search, and spectral information from the whole DSA-2000 band will be useful for determining whether components are different sources or multiple images. Jackson & Browne (2006) show that combining astrometric data from radio and optical surveys can significantly improve the efficiency of lens searches. If the optical emission is dominated by the deflector galaxy then there will exist an offset between the centroid position of the optical and radio sources in a lens system. This offset was exploited to find lenses with separation down to  $\sim 1''$  even with the poor  $5''$  resolution of the Faint Images of the Radio Sky at Twenty-one centimeters (FIRST) survey. They predict that this effect will become more efficient at lower radio fluxes because the optical



flux is more likely to be dominated by the deflector galaxy. Given the sensitivity of the DSA-2000 and its significant overlap with current and planned large surveys in other wavelengths, this could prove to be a very effective way of overcoming the limitations of its PSF. Regardless, exploiting the extra information from overlap with other surveys will be crucial for any lens search in the radio.

Machine learning models have been successfully used to discover many new candidate lens systems. Convolutional Neural Networks (CNNs) in particular are effective at classifying astronomical images. The main disadvantage with CNNs and other supervised learners is the need for large realistic training sets. Using CNNs on simulated data for the International LOFAR Telescope (ILT) at 150 MHz, [Rezaei et al. \(2022\)](#) are able to recover over 90% of galaxy-size lenses with a false-positive rate of only 0.008%. They find that a strong  $20\sigma$  detection and large separation  $\theta_E \geq 3/2$  beam size (stricter than the discoverable limit imposed in Section 2.2) are necessary for reliable identification with the CNN. Incorporating superresolution models into the lens-finding routine would significantly increase the yield of such a CNN, especially at high S/N. Resolving lenses down to  $\theta_E \approx 0.5''$  with would enable the same level of accuracy as in [Rezaei et al. \(2022\)](#). Simulating accurate DSA-2000 lenses and training models for identifying them is a goal of our future work. The SKA-mid will already have sufficient resolution for these purposes, making CNNs an attractive option for lens identification in its all-sky survey.

The main limitation of any ML-based approach to group/cluster lens finding is the difficulty of creating realistic training sets. The irregularity of group/cluster lensing potentials may require building a forward-modelled training set from ray-tracing in large cosmological magnetohydrodynamical simulations such as TNG-Cluster, which should have a heterogeneous population of massive clusters ([Nelson et al. 2024](#)). More generally, a realistic training set of strong lenses across scales could be produced with radio source samples from T-RECS and a deflector population drawn from cosmological simulations.

#### 4 MULTIWAVELENGTH SYNERGIES

Acquiring redshifts for lensed galaxies and deflectors is critical for the application of strong lensing to cosmology and astrophysics. We consider here how well we could do in the absence of targeted follow-up observations, capitalizing on the suite of large survey telescopes that will be operating in the mid- to late-2020s.

**DSA-2000 spectroscopic HI survey** In addition to the cadenced all-sky survey, the DSA-2000 will undertake a large spectroscopic HI survey over the full visible sky ( $\text{Dec} > -30^\circ$ ) ([Hallinan et al. 2019](#)). This is expected to produce  $\sim 10^6$  HI galaxies at  $z < 1$ . Most deflectors will be massive elliptical galaxies with limited 21 cm emission, but a sub-set of early-type galaxies with  $n_H \geq 10^{20} \text{ cm}^{-2} z_d^{-2}$  will be detected. Some late-type deflector galaxies will have enough cold gas to obtain a redshift. Additionally, 21 cm absorption in the inner CGM of deflector galaxies may be present in the lensed source’s continuum spectrum, providing a measurement of cold gas along different sightlines of the same CGM (see [Rudie et al. \(2019\)](#) for a similar application in lensed quasar systems). Thus, some deflector galaxies will have a spectroscopic redshift without any external O/IR data. Of the  $\sim 10^6$  HI galaxies detected by the DSA-2000 in emission, we find that only a handful will be strongly lensed, due to their shallow redshift distribution. Spectroscopic radio observations will not provide a significant portion of redshifts required for our purposes, but may be a minority of interesting deflectors.

**The Dark Energy Spectroscopic Instrument (DESI)** will produce

redshifts of  $\sim 40$  million galaxies and quasars ([DESI Collaboration et al. 2016](#); [Dey et al. 2019](#)). Its 3 yr public data release is expected before the DSA-2000’s first light. DESI’s Bright Galaxy Survey (BGS) targets galaxies with  $r$ -band magnitudes brighter than 19.5. For the luminous red galaxies (LRGs), emission line galaxies (ELGs), and quasars, the depth will be  $r \approx 23$ . Each class of target will have a different redshift distribution, but together they will provide a rich catalog of spectroscopic redshifts for deflectors in the lensing systems discovered by DSA-2000. The BGS and LRG samples will be over-represented as deflector galaxies, whereas the ELG and QSO samples may make up a small fraction of lensed DSA-2000 sources. ELGs, by definition, have strong emission lines indicative of star formation, which produce synchrotron radiation detectable by radio surveys. Some of these will be strongly lensed star-forming radio galaxies with  $S_\nu$  above  $5 \mu\text{Jy}$ . Still, we do not expect more than a small minority of the radio continuum lenses to be detected in DESI due to the relative number of total sources.

**SPHEREx** is a near-infrared space mission expected to launch before Spring 2025. It will map the full  $4\pi$  sr sky with 6 arcsecond pixels and 96 color bands, producing a catalog of hundreds of millions of galaxies with “spectro-photometric redshifts” ([Doré et al. 2018](#)). Although its PSF is too large to discover strong lenses directly, the galaxy catalog will be valuable for obtaining reliable redshifts of both deflectors and lensed galaxies.

**The Rubin Observatory** will find billions of galaxies in its Legacy Survey of Space and Time (LSST) ([Ivezić et al. 2019](#)). Most of these galaxies will be at  $z_s \lesssim 1.5$  ([Collaboration et al. 2021](#)), providing an excellent deflector catalog for the DSA-2000 lens candidates. In the DSA-2000/LSST overlapping footprint between  $-30$  and  $+30$  Declination, we find that a significant fraction of deflectors and several thousand lensed sources in the DSA-2000 sample will have photometric redshifts from the Rubin Observatory.

**Roman** The High Latitude Spectroscopic Survey (HLSS) is expected to detect 10 million galaxies in  $H\alpha$  between  $1 < z < 2$  and  $\sim 2$  million [OIII] galaxies at  $z = 2 - 3$  using the near-IR grism and wide-field camera ([Wang et al. 2022](#)). *Roman’s*  $2,000 \text{ deg}^2$  footprint will be fully mapped by DSA-2000. With a dust-attenuated  $H\alpha$  flux higher than  $10^{-16} \text{ erg s}^{-1} \text{ cm}^{-2}$ , several million of these galaxies will be detectable at GHz frequencies at  $> 5 \mu\text{Jy}$  ([Murphy et al. 2011](#)). Assuming a mean lensing optical depth of  $5 \times 10^{-4}$ , this suggests that  $\mathcal{O}(10^3)$  will be strongly lensed and detected by both the DSA-2000 and *Roman*, the latter providing  $0.1''$  resolution and a source redshift.

**Euclid** is a visible and near-infrared space telescope that launched in July 2023 ([Collaboration et al. 2024](#)). Its large photometric survey will find over one billion galaxies, with a spectroscopic survey that will obtain accurate redshifts for  $\sim 30$  million galaxies mostly at  $0.9 < z < 1.8$ . Euclid and the DSA-2000 share over  $10,000 \text{ deg}^2$  of sky, providing an excellent sample of photometric and spectroscopic redshifts of lens systems.

#### 5 STRONG LENSING APPLICATIONS

A key limitation of strong lensing science is the small number of known systems, especially at radio wavelengths. We discuss the impact that the large expected number of radio lenses and their multi-wavelength counterparts will have on several important applications of strong lensing.

### 5.1 Time-delay cosmography & $H_0$

Light from multiple images in a gravitational lens will reach the observer at different times. For continuum sources, we do not observe the difference in arrival times, but transients or time-variable sources allow us to measure the time delay. This time delay is due to a difference in path lengths and gravitational time dilation near the deflector. As such, the time delay encodes information about the geometry of the universe, and is inversely proportional to  $H_0$  (Oguri 2019). Much work has been dedicated to measuring these time delays and using them to constrain  $H_0$  (Treu & Marshall 2016; Birrer et al. 2024). The HOLiCOW project has measured  $H_0$  to 2.4%, which is independent of and competitive with state-of-the-art  $H_0$  constraints (Wong et al. 2019). A large increase in the number of measurable time-delay systems will allow even tighter constraints and could help settle the current Hubble tension.

We estimate the number of lensed variable AGN that will be useful for measuring  $H_0$  in the DSA-2000. To first order, all blazars (FSRQs and BLLacs) are inherently variable,  $\sim 10^3$  of which will be discoverable as lenses in DSA-2000 data (Table 1). However, several factors complicate our ability to use them for time delay measurements; we would like to know how many will be in a "gold sample" for which the time-delay can be reliably determined. To date, the most extensive study of radio AGN variability is the OVRO 40 m blazar monitoring campaign. Since 2007 this program has monitored around 1500 blazars with a cadence of two weeks (Richards et al. 2011). Richards et al. (2011) provides distributions of the intrinsic modulation index, a measure of the relative intrinsic variability of the AGN, for FSRQs and BLLacs. The DSA-2000 will measure flux variability at the level of a few percent, but to be conservative we consider candidates with  $\geq 10\%$  variability. We also want sources with a strong detection, so we chose sources with flux  $\geq 20\sigma_n = 10 \mu\text{Jy}$ . The OVRO blazars are monitored at 15 GHz but we expect lower variability at 1.4 GHz. Fan, J. H. et al. (2007) find that blazars are about 20% less variable at 4.8 GHz than 14.5 GHz. Sotnikova et al. (2024) find that radio AGN at 22.3 GHz are about 35% more variable than at 2.3 GHz, although there is little difference between 11.2 GHz and 2.3 GHz. We assume that the mean modulation index drops by 40% from the OVRO 40 m data to 1.4 GHz for the DSA-2000. Further, for multiple images, we need at least two of the images to be bright enough to measure the time delay so we use the magnification bias of the fainter image. With these restrictions, the OVRO data, and our lens model, we estimate that there will be  $68 \pm 30$  lensed FSRQs and  $23 \pm 10$  lensed BLLacs with sufficient brightness, variability, and image separation to measure time delays. The same analysis for the SKA-mid gives  $120 \pm 50$  and  $43 \pm 16$  lensed FSRQs and BLLacs.

Of the lensed AGN, the most useful systems for time delay analysis will be those that have four or more images because they allow for multiple constraints on the time delay. A SIS is only capable of creating two images and a spherical NFW can make three, but factors such as ellipticity, irregularities in the lens potential, and external environments of real halos will allow a number of these systems to make four or more images. The fraction of quad galaxy-QSO lenses predicted in Rubin-LSST is  $\sim 10\text{-}15\%$  (Oguri & Marshall 2010; Yue et al. 2022a). However, of the statistically complete CLASS sample, 5 out of 13 lensed blazars were quadruply imaged and one had six images (B1933+503 has two sets of quadruply imaged sources Sykes et al. (1998)). Therefore we can expect 100–400 quadruply-lensed blazars in the DSA-2000 all-sky survey and about twice as many in the SKA-mid, roughly 10% of which may be used in practice for measuring  $H_0$ . We note that quad systems often have higher external shear due to their preponderance of group or cluster environments,

which results in an added systematic in lens modeling (Holder & Schechter 2003).

Wong et al. (2019) reach a 2.4% measurement of  $H_0$  with a sample of 6 lensed quasars, and predict that around 40 lenses are needed to constrain  $H_0$  to within 1%. Jee et al. (2016) argue that with a well-defined sample of quadruply imaged quasars, and combining time-delay distances and velocity dispersion measurements to estimate angular diameter distances within 5%,  $H_0$  can be measured to the same precision as Planck with as few as 10 systems. Napier et al. (2023) reach a 10% measurement with three galaxy clusters, and estimate that roughly 50 will be needed for a sub 1% constraint, assuming that modeling uncertainties can be reduced in coming years. While we expect uncertainty to decrease significantly with a larger sample of lensed quasars, there are several systematics that must be kept under control for an accurate measurement. Namely, an accurate redshift measurement is necessary, ideally of both the source and deflector, as well as precise measurements of the time delay, complete sampling over many cycles of the time delay to negate contamination from micro-lensing, accurate lens models, and constraints on any line of sight structures. If we assume that all of the lenses in our gold sample can be modeled to the accuracy of the HOLiCOW sample – a roughly 6% combined uncertainty on the time delay, mass model, and line of sight contribution for each lens – then a sample of  $\sim 100$  lensed quasars would give about a 0.6% constraint on  $H_0$ . This is of course not possible with the DSA-2000 or SKA-mid alone but will require dedicated follow-up at multiple wavelengths. As discussed in Section 4, we expect that a significant minority of lenses should have redshifts available in other concurrent public surveys. Interesting subsamples of lenses will require targeted follow-up for both mass modeling and spectroscopic redshifts.

The DSA-2000's cadenced all-sky survey will image each field above  $-30$  Dec once every 4 months. Typical time delays for galaxy, group, and cluster lenses in our model are a month or less, several months, and a year or more respectively (Oguri et al. 2002). Special systems could therefore be visited with a higher cadence, similar to how pulsar fields will be visited regularly for timing experiments.

So far we have only considered lensed blazars for time delay measurements, which are desirable because of their characteristic variability and compact emission regions. Lensed transients will also be useful for time delay measurements, provided that they are detected early and monitored closely. The variability of radio emission from TDEs is too slow to make them useful for this application (on-axis jetted TDEs can have shorter rise times, but they are significantly rarer such that we do not expect any lensed jetted TDEs in upcoming radio surveys), but SNe have faster rise times. We expect  $O(1)$  lensed radio ccSNe per year in the DSA-2000 and  $O(10)$  in the SKA-mid that can be used for  $H_0$  measurements.

### 5.2 Dark Matter Structure

Gravitational lensing has been very useful for determining the structure of galaxies, groups, and clusters at cosmological distances and distinguishing between dark matter models (see Vegetti et al. (2024); Natarajan et al. (2024) for a review). The best of these studies use high-resolution HST images, but radio observations also played a pivotal early role. Cohn et al. (2001) used the 10-image CLASS lens B1933+503, which provides many more constraints than usual, to determine the density profile of the deflecting galaxy, finding it close to isothermal. Wucknitz et al. (2004) find the same for B0218+357. Dalal & Kochanek (2002) used radio observations of flux ratio anomalies between multiple images to constrain the mass fraction of dark matter substructure to 2%. Radio observations are especially

suitable for this type of study because they are less susceptible to micro-lensing (Koopmans et al. 2003; Kochanek & Dalal 2004). Despite this, dark matter studies with radio lenses have been limited for many years by the small sample size (Vegetti et al. 2024). Because resolution is a key factor in the ability to accurately model mass distributions or detect substructure, the DSA-2000 alone will not be able to use lens systems to study dark matter. Its main utility will come from identifying huge numbers of systems for detailed follow-up. The extraordinary resolution of the ngVLA on a large sample of lenses selected by the DSA-2000 will revolutionize this field. In the more immediate future, the SKA will also provide enough resolution for these studies in their overlapping sky coverage.

Another exciting application of lensing is using a central image to study small scales near the centers of galaxies (Treu 2010; McKean et al. 2015; Shajib et al. 2024). A SIS lens only forms two images, but for realistic galaxy profiles a highly demagnified image is expected to form at the center of the image configuration. This image will be sensitive to the mass contained within very small distances of the deflector’s center, and so can be used to study supermassive black holes at cosmological distances. This is especially suited for radio wavelengths because in many cases the deflector will be radio-quiet allowing the center image to be detected. Because the center image is highly demagnified, only sensitive radio surveys such as the DSA-2000 will be able to reliably identify them. At least one such central image has been detected in the radio with brightness  $\sim 0.8$  mJy at 8.46 GHz (Winn et al. 2004), so we can likely expect  $O(10^2)$  or more with the DSA-2000. A main challenge will be disentangling the faint emission of the central image from the other images. For groups and clusters, whose inner density profiles are shallower than isothermal, central images are more common and often less demagnified. The very inner profiles of groups/clusters can thus be studied, which are hard to constrain with images near the Einstein radius alone. These central images will be easier to identify because the other images will be farther away (although many clusters have large central elliptical galaxies emitting in the radio that will obscure the image).

### 5.3 Polarization

Measuring full Stokes information of gravitationally lensed signals offers insight into the source plane because polarization is not affected by gravitational potentials. This is an advantage of radio surveys, where polarization information is often stored and Faraday rotation measure (RM) can be measured. This enables us to study propagation effects along different sightlines for lensed objects. For example, Mao et al. (2017) used the VLA to measure the polarization properties of two lensed images of CLASS B1152+199, finding a large difference in RM ( $+9.7 \pm 0.5 \text{ rad m}^{-2}$  for image “A” and  $+517 \pm 3 \text{ rad m}^{-2}$  for image “B”), which is due to the magnetized plasma in the lens galaxy’s interstellar medium.

The DSA-2000 will have the ability to measure full polarization information for any source it detects, with a maximum  $|RM|$  of roughly  $10^4 \text{ rad m}^{-2}$ . Compact sources such as Blazars (and especially BL Lac objects) can show significant polarization fractions at 1 GHz. Assuming a  $50\sigma$  detection threshold in total power, we estimate that the DSA-2000 could detect Stokes Q and U for 5-10 million AGN in its 5 year continuum survey. Using the empirical CLASS lensing optical depth and image separation cut, we take  $\tau_{AGN} \approx 5 \times 10^{-4}$ . We estimate that the DSA-2000 could find  $O(10^3)$  strong lenses for which polarization properties could be used to model the lens distribution and study magnetic fields at cosmological distances.

### 5.4 Other applications

In addition to constraining  $H_0$ , time-delay measurements are weakly sensitive to other cosmological parameters, such as  $\Omega_m$ ,  $\Omega_\Lambda$ , and the dark energy equation of state parameter  $w$  (Natarajan et al. 2024). Cluster lenses are used for studying dark energy as well (Macciò 2005; Gilmore & Natarajan 2009; Jullo et al. 2010). A large influx in measured time delays and observed cluster lenses with the DSA-2000 will allow better constraints on these cosmological parameters. Lenses are also commonly used as “nature’s telescopes”. The magnification of background sources allows very distant galaxies to be studied even by smaller telescopes (Jackson 2011). This is especially true for group/cluster lenses, where we expect the magnifications to be larger (Robertson et al. 2020). We expect to see  $O(10^4)$  lenses with  $z_s > 5$  in the DSA-2000 (figure 4), many of which will be group and cluster lenses due to their high magnifications. These high redshift sources will provide insight into the population of radio sources in the early universe. Lensing statistics can also be used to test cosmological models. The abundance of giant arcs in cluster lenses was a topic of much debate in the past few decades (Meneghetti et al. 2013). Similarly, the rate of GGSL events in clusters may be in tension with the  $\Lambda$ CDM (Meneghetti et al. 2020; Meneghetti, Massimo et al. 2022; Tokayer et al. 2024). These studies require a large sample of lenses for accurate statistics, which is only now becoming possible with large surveys such as the DSA-2000.

## 6 CONCLUSIONS

In this paper, we forecast expected strong lensing rates in the upcoming DSA-2000 and SKA-mid wide-field radio surveys. We first provide empirical estimates based on previous surveys and simulations, and then develop a detailed forward model that accounts for the source and deflector populations, finding them to be in good agreement. Notably, we model the expected number of galaxy group and cluster scale lenses because these systems will be easily discovered due to their wide angular separations. We find that both the DSA-2000 and the SKA-mid will discover roughly  $10^5$  strong lens systems. We discuss strategies for identifying these lenses in the data, which will all benefit from emerging superresolution techniques. Finally, we discuss the scientific application of the huge numbers of lenses that will be discovered by these surveys. One of the most exciting applications is  $H_0$  cosmography with variable and transient sources. The DSA-2000 and SKA-mid will discover about 100 and 200 lensed flat spectrum AGN with  $>10\%$  variability respectively, as well as about  $O(1)$  and  $O(10)$  lensed transients per year. With dedicated multi-wavelength follow up these systems could be used to constrain  $H_0$  to within 1%. The new lens systems will also be useful for studying the distribution of dark matter at cosmological distances, among other applications.

## ACKNOWLEDGEMENTS

We are grateful to Schmidt Sciences for supporting Samuel McCarty as a Summer Undergraduate Research Fellow at Caltech. We thank Kim-Vy Tran, Tony Readhead, and Tommaso Treu for helpful conversations on strong lensing, as well as Paul Schechter for insights into quad systems.

**DATA AVAILABILITY**

We have placed a reproduction package on the public GitHub repository available at <https://github.com/smmccrty/radiolensing>.

**REFERENCES**

- Aghabiglou A., Chu C. S., Dabbech A., Wiaux Y., 2024, *ApJS*, 273, 3
- Alonso D., Ferreira P., 2015, *Physical Review D*, 92
- Alzubaidi L., et al., 2021, *Journal of big Data*, 8, 1
- Auger M. W., Fassnacht C. D., Abrahamse A. L., Lubin L. M., Squires G. K., 2007, *The Astronomical Journal*, 134, 668
- Barroso J. A. A., et al., 2024, Euclid: The Early Release Observations Lens Search Experiment ([arXiv:2408.06217](https://arxiv.org/abs/2408.06217)), <https://arxiv.org/abs/2408.06217>
- Bennett C. L., Lawrence C. R., Burke B. F., Hewitt J. N., Mahoney J., 1986, *ApJS*, 61, 1
- Bietenholz M. F., Bartel N., Argo M., Dua R., Ryder S., Soderberg A., 2021, *The Astrophysical Journal*, 908, 75
- Birrer S., et al., 2024, *Space Sci. Rev.*, 220, 48
- Bonaldi A., Bonato M., Galluzzi V., Harrison I., Massardi M., Kay S., De Zotti G., Brown M. L., 2018, *Monthly Notices of the Royal Astronomical Society*, 482, 2
- Braun R., Bonaldi A., Bourke T., Keane E., Wagg J., 2019, Anticipated Performance of the Square Kilometre Array – Phase 1 (SKA1) ([arXiv:1912.12699](https://arxiv.org/abs/1912.12699)), <https://arxiv.org/abs/1912.12699>
- Browne I. W. A., et al., 2003, *Monthly Notices of the Royal Astronomical Society*, 341, 13–32
- Böhringer, Hans Chon, Gayoung Fukugita, Masataka 2017, *A&A*, 608, A65
- Cabanac, R. A. et al., 2007, *A&A*, 461, 813
- Cendes Y., et al., 2023, Ubiquitous Late Radio Emission from Tidal Disruption Events ([arXiv:2308.13595](https://arxiv.org/abs/2308.13595)), <https://arxiv.org/abs/2308.13595>
- Cohn J. D., Kochanek C. S., McLeod B. A., Keeton C. R., 2001, *The Astrophysical Journal*, 554, 1216
- Collaboration T. L. D. E. S., et al., 2021, The LSST Dark Energy Science Collaboration (DESC) Science Requirements Document ([arXiv:1809.01669](https://arxiv.org/abs/1809.01669)), <https://arxiv.org/abs/1809.01669>
- Collaboration E., et al., 2024, Euclid. I. Overview of the Euclid mission ([arXiv:2405.13491](https://arxiv.org/abs/2405.13491)), <https://arxiv.org/abs/2405.13491>
- Collett T. E., 2015, *The Astrophysical Journal*, 811, 20
- Connor L., Ravi V., 2023, *MNRAS*, 521, 4024
- Connor L., Bouman K. L., Ravi V., Hallinan G., 2022, *Monthly Notices of the Royal Astronomical Society*, 514, 2614–2626
- Cordes J. M., Chatterjee S., 2019, *ARA&A*, 57, 417
- Coupon, J. et al., 2009, *A&A*, 500, 981
- DESI Collaboration et al., 2016, *arXiv e-prints*, p. [arXiv:1611.00036](https://arxiv.org/abs/1611.00036)
- Dalal N., Kochanek C. S., 2002, *The Astrophysical Journal*, 572, 25–33
- Dey A., et al., 2019, *AJ*, 157, 168
- Diego J. M., et al., 2023, *A&A*, 672, A3
- Doré O., et al., 2018, Science Impacts of the SPHEREx All-Sky Optical to Near-Infrared Spectral Survey II: Report of a Community Workshop on the Scientific Synergies Between the SPHEREx Survey and Other Astronomy Observatories ([arXiv:1805.05489](https://arxiv.org/abs/1805.05489)), <https://arxiv.org/abs/1805.05489>
- Dutton A. A., Macciò A. V., 2014, *Monthly Notices of the Royal Astronomical Society*, 441, 3359
- Dyer C. C., Shaver E. G., 1992, *ApJ*, 390, L5
- Fan, J. H. et al., 2007, *A&A*, 462, 547
- Fedeli, C. Meneghetti, M. Gottlöber, S. Yepes, G. 2010, *A&A*, 519, A91
- Ferrami G., Wyithe J. S. B., 2024, *Monthly Notices of the Royal Astronomical Society*, 532, 1832–1848
- Fleury P., Larena J., Uzan J.-P., 2021, *Journal of Cosmology and Astroparticle Physics*, 2021, 024
- Gavazzi R., Treu T., Rhodes J. D., Koopmans L. V. E., Bolton A. S., Burles S., Massey R. J., Moustakas L. A., 2007, *ApJ*, 667, 176
- Ghirlanda G., et al., 2013, *Monthly Notices of the Royal Astronomical Society*, 435, 2543
- Ghirlanda G., et al., 2014, *Publications of the Astronomical Society of Australia*, 31, e022
- Gilmore J., Natarajan P., 2009, *Monthly Notices of the Royal Astronomical Society*, 396, 354
- Gladders M. D., Hoekstra H., Yee H. K. C., Hall P. B., Barrientos L. F., 2003, *The Astrophysical Journal*, 593, 48
- Greenfield P. D., Roberts D. H., Burke B. F., 1985, *ApJ*, 293, 370
- Hallinan G., et al., 2019, The DSA-2000 – A Radio Survey Camera ([arXiv:1907.07648](https://arxiv.org/abs/1907.07648)), <https://arxiv.org/abs/1907.07648>
- Han J. J., et al., 2023, *arXiv e-prints*, p. [arXiv:2306.11784](https://arxiv.org/abs/2306.11784)
- Holder G. P., Schechter P. L., 2003, *The Astrophysical Journal*, 589, 688–692
- Ivezić Ž., et al., 2019, *ApJ*, 873, 111
- Jackson N., 2011, *ApJ*, 739, L28
- Jackson N., Browne I. W. A., 2006, *Monthly Notices of the Royal Astronomical Society*, 374, 168
- Lee I., Komatsu E., Suyu S., Huterer D., 2016, *Journal of Cosmology and Astroparticle Physics*, 2016, 031–031
- Jullo E., Natarajan P., Kneib J.-P., D’Aloisio A., Limousin M., Richard J., Schimd C., 2010, *Science*, 329, 924–927
- Kader Z., et al., 2022, *Phys. Rev. D*, 106, 043016
- Klypin A., Yepes G., Gottlöber S., Prada F., Heß S., 2016, *Monthly Notices of the Royal Astronomical Society*, 457, 4340
- Kochanek C. S., Dalal N., 2004, *The Astrophysical Journal*, 610, 69–79
- Kool E. C., et al., 2023, *Nature*, 617, 477
- Koopmans L. V. E., et al., 2003, *The Astrophysical Journal*, 595, 712
- Koopmans L. V. E., et al., 2009, *ApJ*, 703, L51
- Korytov D., et al., 2019, *The Astrophysical Journal Supplement Series*, 245, 26
- Lacy M., et al., 2020, *Publications of the Astronomical Society of the Pacific*, 132, 035001
- Lemon C., et al., 2023, Searching for strong gravitational lenses ([arXiv:2310.13466](https://arxiv.org/abs/2310.13466)), <https://arxiv.org/abs/2310.13466>
- Leung C., et al., 2022, *Phys. Rev. D*, 106, 043017
- Li L.-X., Ostriker J. P., 2002, *The Astrophysical Journal*, 566, 652
- Li R., Shu Y., Wang J., 2018, *Monthly Notices of the Royal Astronomical Society*, 480, 431
- Lien A., Chakraborty N., Fields B. D., Kembal A., 2011, *The Astrophysical Journal*, 740, 23
- Lim B., Son S., Kim H., Nah S., Mu Lee K., 2017, in *Proceedings of the IEEE Conference on Computer Vision and Pattern Recognition (CVPR) Workshops*.
- Limousin, M. et al., 2009, *A&A*, 502, 445
- Macciò A. V., 2005, *Monthly Notices of the Royal Astronomical Society*, 361, 1250
- Mahdi H. S., van Beek M., Elahi P. J., Lewis G. F., Power C., Killedar M., 2014, *Monthly Notices of the Royal Astronomical Society*, 441, 1954
- Mandelbaum R., Seljak U., Cool R. J., Blanton M., Hirata C. M., Brinkmann J., 2006, *Monthly Notices of the Royal Astronomical Society*, 372, 758
- Mao S. A., et al., 2017, *Nature Astronomy*, 1, 621–626
- Mars M., Betcke M. M., McEwen J. D., 2024, *arXiv e-prints*, p. [arXiv:2405.08958](https://arxiv.org/abs/2405.08958)
- Martinez M. N., Gordon Y. A., Bechtol K., Cartwright G., Ferguson P. S., Gorsuch M., 2024, Finding Lensed Radio Sources with the VLA Sky Survey ([arXiv:2404.09954](https://arxiv.org/abs/2404.09954)), <https://arxiv.org/abs/2404.09954>
- Massey R., Kitching T., Richard J., 2010, *Reports on Progress in Physics*, 73, 086901
- Matthews A. M., Condon J. J., Cotton W. D., Mauch T., 2021, *The Astrophysical Journal*, 909, 193
- McKean J. P., et al., 2015, Strong gravitational lensing with the SKA ([arXiv:1502.03362](https://arxiv.org/abs/1502.03362)), <https://arxiv.org/abs/1502.03362>
- Meneghetti, Massimo et al., 2022, *A&A*, 668, A188
- Meneghetti M., Bartelmann M., Dahle H., Limousin M., 2013, *Space Science Reviews*, 177, 31
- Meneghetti M., et al., 2020, *Science*, 369, 1347–1351
- More A., Cabanac R., More S., Alard C., Limousin M., Kneib J.-P., Gavazzi R., Motta V., 2012, *The Astrophysical Journal*, 749, 38

- Murphy E. J., et al., 2011, *ApJ*, **737**, 67
- Myers S. T., et al., 2003, *Monthly Notices of the Royal Astronomical Society*, **341**, 1–12
- Napier K., Sharon K., Dahle H., Bayliss M., Gladders M. D., Mahler G., Rigby J. R., Florian M., 2023, *The Astrophysical Journal*, **959**, 134
- Natarajan P., Williams L. L. R., Bradač M., Grillo C., Ghosh A., Sharon K., Wagner J., 2024, *Space Science Reviews*, **220**, 19
- Navarro J. F., Frenk C. S., White S. D. M., 1997, *ApJ*, **490**, 493
- Nelson D., Pillepich A., Ayromlou M., Lee W., Lehle K., Rohr E., Truong N., 2024, *A&A*, **686**, A157
- Newman A. B., Treu T., Ellis R. S., Sand D. J., Nipoti C., Richard J., Jullo E., 2013, *The Astrophysical Journal*, **765**, 24
- Newman A. B., Ellis R. S., Treu T., 2015, *The Astrophysical Journal*, **814**, 26
- Oguri M., 2006, *MNRAS*, **367**, 1241
- Oguri M., 2019, *Reports on Progress in Physics*, **82**, 126901
- Oguri M., Marshall P. J., 2010, *Monthly Notices of the Royal Astronomical Society*, **405**, 2579
- Oguri M., Taruya A., Suto Y., 2001, *The Astrophysical Journal*, **559**, 572–583
- Oguri M., Taruya A., Suto Y., Turner E. L., 2002, *The Astrophysical Journal*, **568**, 488
- Petroff E., Hessels J. W. T., Lorimer D. R., 2019, *A&ARv*, **27**, 4
- Puchwein E., Hilbert S., 2009, *Monthly Notices of the Royal Astronomical Society*, **398**, 1298
- Refsdal S., 1964, *MNRAS*, **128**, 307
- Rezaei S., McKean J. P., Biehl M., de Roo W., Lafontaine A., 2022, *Monthly Notices of the Royal Astronomical Society*, **517**, 1156
- Richards J. L., et al., 2011, *ApJS*, **194**, 29
- Robertson A., Smith G. P., Massey R., Eke V., Jauzac M., Bianconi M., Ryczanowski D., 2020, *Monthly Notices of the Royal Astronomical Society*, **495**, 3727
- Rudie G. C., Steidel C. C., Pettini M., Trainor R. F., Strom A. L., Hummels C. B., Reddy N. A., Shapley A. E., 2019, *ApJ*, **885**, 61
- Selina R. J., et al., 2018a, in Murphy E., ed., *Astronomical Society of the Pacific Conference Series Vol. 517, Science with a Next Generation Very Large Array*. p. 15 ([arXiv:1810.08197](https://arxiv.org/abs/1810.08197)), [doi:10.48550/arXiv.1810.08197](https://doi.org/10.48550/arXiv.1810.08197)
- Selina R. J., et al., 2018b, in Marshall H. K., Spyromilio J., eds, *Society of Photo-Optical Instrumentation Engineers (SPIE) Conference Series Vol. 10700, Ground-based and Airborne Telescopes VII*. p. 107001O ([arXiv:1806.08405](https://arxiv.org/abs/1806.08405)), [doi:10.1117/12.2312089](https://doi.org/10.1117/12.2312089)
- Shajib A. J., et al., 2024, *Strong Lensing by Galaxies* ([arXiv:2210.10790](https://arxiv.org/abs/2210.10790)), <https://arxiv.org/abs/2210.10790>
- Sotnikova Y., et al., 2024, *Galaxies*, **12**, 25
- Sykes C. M., et al., 1998, *Monthly Notices of the Royal Astronomical Society*, **301**, 310
- Tokayer Y. M., Dutra I., Natarajan P., Mahler G., Jauzac M., Meneghetti M., 2024, *The galaxy-galaxy strong lensing cross section and the internal distribution of matter in LambdaCDM substructure* ([arXiv:2404.16951](https://arxiv.org/abs/2404.16951)), <https://arxiv.org/abs/2404.16951>
- Treu T., 2010, *ARA&A*, **48**, 87
- Treu T., Marshall P. J., 2016, *The Astronomy and Astrophysics Review*, **24**
- Vegetti S., et al., 2024, *Space Science Reviews*, **220**, 58
- Walsh D., Carswell R. F., Weymann R. J., 1979, *Nature*, **279**, 381
- Wang Y., et al., 2022, *The Astrophysical Journal*, **928**, 1
- Wang C., et al., 2023, *Monthly Notices of the Royal Astronomical Society*, **527**, 1580
- Weiner C., Serjeant S., Sedgwick C., 2020, *Research Notes of the AAS*, **4**, 190
- Williams L. L. R., Navarro J. F., Bartelmann M., 1999, *The Astrophysical Journal*, **527**, 535
- Winn J. N., Rusin D., Kochanek C. S., 2004, *Nature*, **427**, 613
- Wong K. C., et al., 2019, *Monthly Notices of the Royal Astronomical Society*, **498**, 1420–1439
- Wucknitz O., Biggs A. D., Browne I. W. A., 2004, *Monthly Notices of the Royal Astronomical Society*, **349**, 14–30
- Wucknitz O., Spitler L. G., Pen U. L., 2021, *A&A*, **645**, A44
- Wyithe J. S. B., Turner E. L., Spergel D. N., 2001, *The Astrophysical Journal*, **555**, 504
- Yao Y., et al., 2023, *The Astrophysical Journal Letters*, **955**, L6
- Yu J., Fan Y., Yang J., Xu N., Wang Z., Wang X., Huang T., 2018a, *Wide Activation for Efficient and Accurate Image Super-Resolution* ([arXiv:1808.08718](https://arxiv.org/abs/1808.08718)), <https://arxiv.org/abs/1808.08718>
- Yu J., Lin Z., Yang J., Shen X., Lu X., Huang T. S., 2018b, in *Proceedings of the IEEE conference on computer vision and pattern recognition*. pp 5505–5514
- Yue M., Fan X., Yang J., Wang F., 2022a, *The Astronomical Journal*, **163**, 139
- Yue M., Fan X., Yang J., Wang F., 2022b, *The Astrophysical Journal*, **925**, 169
- Zhang K., Ren W., Luo W., Lai W.-S., Stenger B., Yang M.-H., Li H., 2022, *International Journal of Computer Vision*, **130**, 2103
- Zwicky F., 1937, *ApJ*, **86**, 217

This paper has been typeset from a  $\text{\TeX}/\text{\LaTeX}$  file prepared by the author.